

# A new approach to analyzing the spinor wave functions: Effect of strain on the electronic structure and optical transitions in bulk CdSe

A. I. Lebedev\*

*Physics Department, Lomonosov Moscow State University*

(Dated: July 31, 2023)

An approach to analyzing the spinor wave functions that appear in the electronic structure calculations when taking the spin-orbit interaction into account is developed. It is based on the projection analysis of angular parts of wave functions onto irreducible representations of the point group and analysis of the evolution of the energy levels upon the adiabatic turning on the spin-orbit interaction. The technique is illustrated by an example of the changes in the valence band structure in strained bulk CdSe with zinc-blende structure. An analysis of the character of mixing of various branches of the valence band supports the Luttinger–Kohn model of the valence band. It is shown that the above calculations complemented by the Zeeman splitting in a magnetic field make it possible to unambiguously determine the polarization of all optical transitions. Using the spinor wave functions, matrix elements of optical transitions between the valence subbands and the conduction band are calculated.

Keywords: semiconductors, zinc-blende structure, first-principles calculations

## I. INTRODUCTION

Being one of the perturbation theory techniques, the  $\mathbf{k} \cdot \mathbf{p}$  method [1, 2] found wide application in solid state physics. Strictly speaking, the use of this method requires to know the energies of an infinite number of bands and an infinite number of matrix elements. Löwdin [3] proposed a mathematical trick that allowed to project this problem onto a system with a finite number of bands. It is in this truncated form that the  $\mathbf{k} \cdot \mathbf{p}$  method is usually used as an “interpolation scheme” to describe the band structure of semiconductors in the vicinity of a given point of the Brillouin zone. In fact, this method is *semi-empirical* since it borrows all necessary parameters from the experiment. To calculate the dispersion curves, there is no need to know the wave functions; their knowledge becomes necessary when one needs to calculate the matrix elements of optical transitions and the character of their optical polarization.

A detailed comparison of predictions obtained using the first-principles calculations and the  $\mathbf{k} \cdot \mathbf{p}$  method showed that in respect to low-dimensional structures (they will be the subject of our further research), the predictions of the  $\mathbf{k} \cdot \mathbf{p}$  method are characterized by a large number of shortcomings described and analyzed in detail in Refs. [4–8]. First of all, these are errors in the prediction of energies of all subbands except for those that were used as empirical parameters; overestimation of the size effect; impossibility to predict *a full set* of subbands in the conduction band [4, 5] as well in the valence band [7], and to describe optical transitions involving all subbands of the conduction band [7]. The main cause of these errors is the insufficient number of bands taken into account in the calculations, which leads to significant errors in description of dispersion curves. A basis of

eight (including spin) bands is the most commonly used in these calculations. At the same time, as was shown in Ref. [8], it is necessary to take at least 30 bands (including spin) into account for a qualitative description of the band dispersion in GaAs, and its quantitative description requires about 150 bands. When modeling the low-dimensional structures within the  $\mathbf{k} \cdot \mathbf{p}$  method, one more problem arises: their description in the envelope function approximation, which is based on the assumption of smoothness of this function, is formally impossible due to the appearance the Fourier component of the potential that goes beyond the first Brillouin zone. Additional difficulties arise when modeling heterostructures with a strong lattice mismatch. These problems are absent in the first-principles calculations.

The aim of this work was to develop an approach to analyzing the spinor wave functions that would allow one to determine the genesis of various bands in low-dimensional structures. The problem is that due to the size quantization effects and strong mixing of different branches of the electronic spectrum, the identification of electronic states in the valence band of these structures becomes extremely complicated. Since optical transitions that take into account their polarization are determined by the total angular momentum  $j$  and magnetic quantum number  $m_j$  in the initial and final states, it becomes necessary to determine the contributions of states with different  $(j, m_j)$  to the initial and final states. The available programs for an analysis of spinor wave functions (see [9] and the references therein) are usually limited to determining the symmetry of the wave functions; this is absolutely insufficient for determining the genesis and identifying bands.

Cadmium selenide CdSe was chosen as an object on which the proposed approach will be tested as it is a direct-gap semiconductor and has interesting optical properties. A considerable interest in CdSe now is associated with the study of nanoparticles of various shapes made of this material [10–12].

---

\* swan@scon155.phys.msu.ru

In the bulk form, cadmium selenide usually crystallizes in the wurtzite hexagonal structure (space group  $P6_3mc = C_{6v}^4$ ) while its cubic phase with the zinc-blende structure (space group  $F\bar{4}3m = T_d^2$ ) is metastable. However, under certain synthesis conditions, samples can be obtained in the zinc-blende structure. In particular, nanocrystals obtained by chemical route at low temperatures often have this structure.

Calculations of the electronic structure of cubic CdSe and its optical properties in a wide energy range were carried out using OPW, LCAO, empirical pseudopotential, and FP-LAPW methods [13–17]. The  $\mathbf{k} \cdot \mathbf{p}$  method was used to calculate the electronic structure and optical matrix elements in CdSe nanoplatelets [18–20].

## II. CALCULATION TECHNIQUE

Calculations of the electronic structure of bulk CdSe with the zinc-blende structure with taking the spin-orbit interaction into account were carried out from first principles within the density-functional theory using the ABINIT program [21]. The local density approximation (LDA) and PAW pseudopotentials [22] were used in the calculations. The plane wave cutoff energy was 30 Ha (816 eV). The unit cell parameters and atomic positions were relaxed until the forces acting on the atoms became less than  $5 \cdot 10^{-6}$  Ha/Bohr (0.25 meV/Å) while the accuracy of the total energy calculation was better than  $10^{-10}$  Ha. A number of calculations were also performed using the HGH pseudopotentials [23] with a cutoff energy of 60 Ha and the ONCVSP ones [24] with a cutoff energy of 50 Ha.

In real low-dimensional structures—superlattices, nanoplatelets, and nanoheterostructures grown in the [001] direction—the layers are strained, and so their symmetry is tetragonal or lower. This is why we consider CdSe as an active region of such structures and study the properties of CdSe biaxially stretched and biaxially compressed in the  $xy$  plane.

Since the spin-orbit interaction practically does not affect the geometry of structures, the calculations of the equilibrium geometry were carried out without taking spin into account. The band energies and spinor wave functions in the obtained structures were calculated with the spin-orbit interaction turned on. To output the values of the matrix elements of the momentum operator, small changes were added into the code of the ABINIT program. To unambiguously separate optical transitions from the light holes and of split-off holes to the conduction band in  $\sigma$  and  $\pi$  polarizations, a magnetic field was applied parallel to the  $z$  axis of the sample. The possibility of such calculations was recently added into the program [25]. Since these calculations in the ABINIT program are implemented only for norm-conserving pseudopotentials, the HGH and ONCVSP pseudopotentials were used in these calculations.

Using two components of the new approach, namely,

(1) tracing the changes in the energies of bands upon the “adiabatic” turning on the spin-orbit interaction and (2) determining the genesis of the spinor wave functions by expanding their angular parts in terms of irreducible representations of the point group, it becomes possible to identify the bands, trace their evolution, and determine the degree of mixing of various electronic states in them and their symmetry. As far as the author knows, this approach to an analysis of the spinor wave functions have not been used before.

Since CdSe is a direct-gap semiconductor with the band extrema at the  $\Gamma$  point of the Brillouin zone, we will be interested in optical transitions exactly at this point when analyzing its optical properties. Upon a tetragonal distortion of the structure along the  $z$  axis, the FCC Bravais lattice transforms into a body-centered tetragonal Bravais lattice whose translation vectors are rotated by  $45^\circ$  in the  $xy$  plane with respect to the axes of the FCC lattice. Therefore, the directions of the  $\Delta$  and  $\Sigma$  axes in the Brillouin zone are also interchanged with respect to their directions in the cubic structure.

## III. GROUP-THEORETICAL BACKGROUND

As will be shown in Sec. IV A, the valence band of cubic CdSe is mainly composed of the  $p$  orbitals of Se (orbital angular momentum  $l = 1$ ). They will be denoted by  $|X\rangle$ ,  $|Y\rangle$ , and  $|Z\rangle$ . Without taking the spin-orbit interaction into account, the valence band at the  $\Gamma$  point is threefold degenerate and is described by a vector irreducible representation  $T_2$  [26] ( $F_2$  according to Bir and Pikus [27]). When moving away from the  $\Gamma$  point, these bands split into a nondegenerate band of light carriers (with magnetic quantum number  $m = 0$ ) and a doubly degenerate band of heavy carriers (with  $m = \pm 1$ ). As will be shown below, the conduction band originates from the  $s$  states of Se and Cd atoms ( $l = 0$ ), is nondegenerate, and has a symmetry of  $A_1$  ( $\Gamma_1$ ).

When the spin-orbit interaction is turned on, the symmetry of wave functions is described by the irreducible representations of the double group in which the operations of the  $T_d$  point group are supplemented by the transformations of the spin variable. In contrast to five irreducible representations of the  $T_d$  point group at the  $\Gamma$  point, there are three irreducible representations in the double group [26]. They are direct products of representations of the point group and the  $\mathcal{D}_{1/2}$  representation of the rotation group for particles with spin 1/2. In particular,  $\Gamma_6 = \mathcal{D}_{1/2} \otimes A_1$ , and the direct product  $\mathcal{D}_{1/2} \otimes T_2$  is reducible and splits into the sum  $\Gamma_8 \oplus \Gamma_7$ .

Spin-orbit interaction causes a complex mixing of  $|X\rangle$ ,  $|Y\rangle$ , and  $|Z\rangle$  orbitals and results in the lifting of the threefold degeneracy of the valence bands at the  $\Gamma$  point; the bands are split according to their total angular momentum  $j$ . The heavy holes HH ( $j = 3/2$ ,  $m_j = \pm 3/2$ ) and light holes LH ( $j = 3/2$ ,  $m_j = \pm 1/2$ ), which originate genetically from the doubly degenerate band of heavy

carriers with  $m = \pm 1$ , are shifted upwards, and the split-off SO band ( $j = 1/2$ ,  $m_j = \pm 1/2$ ) arising from the nondegenerate band of light carriers with  $m = 0$  shifts downwards. The symmetry of the LH and HH bands which are doubly degenerate at the  $\Gamma$  point is described by the  $\Gamma_8$  irreducible representation of the double group,

the symmetry of the SO band is described by the  $\Gamma_7$  representation, and that of the conduction band is described by the  $\Gamma_6$  representation.

The wave functions of the conduction and three valence bands at the  $\Gamma$  point in a cubic crystal have the form [28–30]:

$$\begin{aligned} \phi_{c1} &= |iS\downarrow\rangle; \quad \phi_{c2} = |iS\uparrow\rangle; \quad \phi_{hh1} = \frac{1}{\sqrt{2}}|(X + iY)\uparrow\rangle; \quad \phi_{hh2} = \frac{1}{\sqrt{2}}|(X - iY)\downarrow\rangle; \\ \phi_{lh1} &= \frac{1}{\sqrt{6}}|(X - iY)\uparrow\rangle + \sqrt{\frac{2}{3}}|Z\downarrow\rangle; \quad \phi_{lh2} = \frac{1}{\sqrt{6}}|(-X + iY)\downarrow\rangle + \sqrt{\frac{2}{3}}|Z\uparrow\rangle; \\ \phi_{so1} &= \frac{1}{\sqrt{3}}|(X - iY)\uparrow\rangle - \frac{1}{\sqrt{3}}|Z\downarrow\rangle; \quad \phi_{so2} = \frac{1}{\sqrt{3}}|(-X + iY)\downarrow\rangle - \frac{1}{\sqrt{3}}|Z\uparrow\rangle \end{aligned} \quad (1)$$

(when choosing the coefficients, we follow the paper [30]). When moving away from the  $\Gamma$  point, the degeneracy of the LH and HH bands is lifted and their mixing occurs.

Biaxial compression or tension of the crystals in the (001) plane lowers their symmetry to  $I\bar{4}m2$  ( $D_{2d}^9$ ) and results in a significant change of their electronic structure. From the group-theoretical point of view, when the symmetry of a crystal is reduced to  $D_{2d}$ , the number of irreducible representations at the  $\Gamma$  point of the point group remain the same (five), but their number in the double group is reduced to two ( $\Gamma_6$  and  $\Gamma_7$ ) [26]. The vector representation  $T_2$  of the point group of the cubic structure becomes reducible:  $T_2 \rightarrow B_2 \oplus E$ . Representations of the double group in the tetragonal structure are obtained as follows:  $\Gamma_6 = \mathcal{D}_{1/2} \otimes A_1$  (conduction band),  $\Gamma_7 = \mathcal{D}_{1/2} \otimes B_2$  (SO band). Direct product  $\mathcal{D}_{1/2} \otimes E$  (light and heavy holes) turns out to be reducible and decomposes into the sum  $\Gamma_6 \oplus \Gamma_7$ . For odd spinor functions originating from  $p$  atomic orbitals, the  $\Gamma_6$  symmetry indicates the heavy holes, and the  $\Gamma_7$  one indicates the light holes [26]. The reducibility of the representation means that under a tetragonal distortion, the degeneracy of the HH and LH bands is lifted at the  $\Gamma$  point ( $\Gamma_8 \rightarrow \Gamma_6 \oplus \Gamma_7$ ). The fact that the states of the LH and SO bands in a strained crystal are described by the same representation ( $\Gamma_7$ ) indicates the possibility of their mixing.

Below, when analyzing the symmetry of spinor wave functions, we will use the projection analysis to determine the expansion coefficients of the angular parts of wave functions in an orthogonal basis of irreducible representations of the point group. In a cubic crystal, all 4th order axes are equivalent, and the projection analysis does not allow to resolve the contributions of bands with different  $m$  at the  $\Gamma$  point. Under a tetragonal strain ( $F\bar{4}3m \rightarrow I\bar{4}m2$ ), the  $z$  direction becomes distinguished, the degeneracy of the  $m = 0$  and  $m = \pm 1$  states is lifted, and unambiguous determination of the fraction of  $|Z\rangle$  states in the LH and SO bands of the  $\Gamma_7$  symmetry using the projection analysis becomes possible. This turns out to be very important for determining the matrix elements

of optical transitions.

While in a cubic semiconductor, in accordance with Eq. (1), the contributions of the  $|X\rangle$ ,  $|Y\rangle$ , and  $|Z\rangle$  orbitals to the SO band are the same (this is a kind of a “cubic reference point” that arises from the equivalence of three directions of a cube), under a tetragonal distortion the  $|X \pm iY\rangle$  and  $|Z\rangle$  states become independent. As will be shown below, the projection analysis finds a strong change in proportions of these states in a strained structure, and since it significantly affects the matrix elements of optical transitions, this makes it possible to change the absorption and luminescence spectra of a semiconductor using the elastic strain.

We note that until now the discussion of the strain effects on the electronic structure of the valence band within the  $\mathbf{k} \cdot \mathbf{p}$  method was usually limited to consideration of the band energies and their dispersions [2, 27, 31]. One of a few papers that has discussed the changes in the wave functions and matrix elements of optical transitions in strained crystals with zinc-blende structure, was the paper [32].

## IV. RESULTS AND THEIR DISCUSSION

### A. Determination of symmetry and genesis of spinor wave functions

We have already noted that the symmetry of the spinor wave functions at the  $\Gamma$  point in tetragonal structures can be either  $\Gamma_6$  or  $\Gamma_7$ . Determination of the symmetry of wave functions and their genesis proved to be not an easy task. The fact is that in programs for electronic structure calculations, only the spatial symmetry of wave functions (given by the point group) is taken into account. This is because in the double group there is always the  $\bar{E}$  operator, which corresponds to a rotation of a crystal by  $360^\circ$  and changes the sign of the wave function to opposite. So, if the spin variable were taken into account, then the resulting wave function would always be identically equal

to zero.

To find the double group representation that describes the symmetry of a given wave function, we analyzed the symmetry of each of its spinor components for  $\mathbf{k} = 0$  averaged in the  $xy$  plane with respect to reflections in the plane passing through the cadmium atom. The components of the wave functions were extracted from the array of wave functions using the `cut3d` program included into the ABINIT software package. Although the  $I4m2$  space group does not contain the indicated symmetry operation, the improper rotation  $S_4$  creates such an operation for the plane-averaged wave function. Even functions correspond to the  $\Gamma_6$  symmetry, odd functions correspond to the  $\Gamma_7$  one. The obtained symmetries of wave functions were confirmed later by calculations of the matrix elements of optical transitions between the valence subbands and the conduction band; they completely agree with the results obtained using the `IrRep` program [9].

As noted above, the existence of only two double group representations means that they can arise from a superposition of four different states: light, heavy, split-off holes, and  $s$ -like states of the conduction band in the initial cubic crystal. To determine the genesis of spinor wave functions, the symmetry of both components of the spinor wave function  $\psi$  for each band was analyzed in respect to all operations  $g$  of the point group  $G = D_{2d}$ . The desired parameters were the values

$$F(g) = \frac{\|g\psi + \psi\|^2 - \|g\psi - \psi\|^2}{4\|\psi\|^2}, \quad (2)$$

which were then decomposed using the character table in an orthogonal basis of irreducible representations of the  $D_{2d}$  point group. The decomposition coefficients

$$a_i = \frac{1}{|G|} \sum_{g \in G} \chi_i(g) \nu_i F(g), \quad (3)$$

where  $|G|$  is the number of elements in the group, and  $\chi_i$  is the character of the  $i$ th representation, determine the contributions of different representations to the analyzed wave function. The factor  $\nu_i$  corrects the scalar product (2) for the dimension of the  $i$ th representation. When performing the analysis, it turned out to be important to choose the position of the reference point in the unit cell in such a way that it coincided with one of the points of high symmetry; in our calculations, it was the  $2(a)$  Wyckoff position. To avoid the problem arising from the degeneracy of components of the spinor wave function at  $\mathbf{k} = 0$ , the analysis was performed for the wave vector shifted along the  $\Sigma$  axis from the  $\Gamma$  point to a distance of about  $0.0005 \text{ \AA}^{-1}$ . [33] As expected, the  $A_1$ ,  $B_2$ , and  $E$  representations appeared in the projections; the projections onto  $A_2$  and  $B_1$  irreducible representations were absent.

An analysis of the projections of the obtained spinor wave functions onto atoms shows that the conduction band of CdSe is composed of 56% of  $s$  orbitals of Se

atoms and 44% of  $s$  orbitals of Cd atoms. The states in the valence band are formed mainly from  $p$  orbitals of Se with an admixture of about 7% of  $d$  states of Cd and 2%  $p$  states of Cd and therefore, according to their genesis, can be classified as light, heavy, and split-off holes. The main problem in interpreting these bands is how to distinguish between light and heavy holes whose projections onto irreducible representations of the point group have the same symmetry ( $E$ ). Since the spin-orbit interaction lifts the twofold degeneracy of the  $E$  level, it is possible, by tracing the change in energies of levels at adiabatic turning on the spin-orbit interaction, [34] and by taking the previously obtained symmetry of bands ( $\Gamma_6$  or  $\Gamma_7$ ) into account, to unambiguously identify the LH and HH subbands (Fig. 1). As for the SO subband, it does not exhibit splitting at turning on the spin-orbit interaction. An additional argument in the analysis can be that the projections of LH and SO bands are always a mixture of  $B_2$  and  $E$  states because of the strong admixture of  $|Z\rangle$  states to wave functions (see Eq. (1)), whereas the HH band has a pure  $E$  symmetry.

An analysis of the projections of spinor wave functions onto irreducible representations of the point group shows that the symmetry of the conduction band (CB) in CdSe is closest to the  $s$  type: the angular part of its wave function  $\Gamma_6$  is projected onto the  $A_1$  representation; the admixture of contributions of other symmetries does not exceed 0.1%. The angular part of the wave functions of HH band with the  $\Gamma_6$  symmetry is projected onto the  $E$  representation; an admixture of wave functions of other symmetries does not exceed 0.1–0.2%. Despite the same symmetry of the CB and HH bands, they have different parity with respect to the inversion and, therefore, they do not mix at the  $\Gamma$  point (their mixing becomes possible at  $\mathbf{k} \neq 0$ ). As expected, the strongest mixing effects at the  $\Gamma$  point are observed for the LH and SO bands, which have the same  $\Gamma_7$  symmetry. In summary, the first-principles calculations confirm the adequacy of assumptions underlying the Luttinger–Kohn valence band model [28].

The evolution of the energies of various branches of the valence band upon the adiabatic turning on the spin-orbit interaction in biaxially compressed and biaxially stretched CdSe crystals is shown in Fig. 1. When the spin-orbit interaction is turned off ( $\lambda_{\text{SO}} = 0$ ), there is already a splitting of bands caused by strain in crystals. When the spin-orbit interaction is turned on, the sequence of bands in a biaxially compressed sample corresponds to its usual order (the upper subband is the heavy holes one, the following subband is the light holes band, and the lowest subband is the split-off band). In biaxially stretched samples, the situation is more interesting. As follows from the figure, the upper energy band (denoted as LH) is genetically derived from the band of the  $B_2$  symmetry with  $m = 0$ , which generates states with a total angular momentum  $j = 1/2$  when the spin-orbit interaction is turned on. This is evidenced by the absence of splitting. When the  $\lambda_{\text{SO}}$  is increased, the frac-

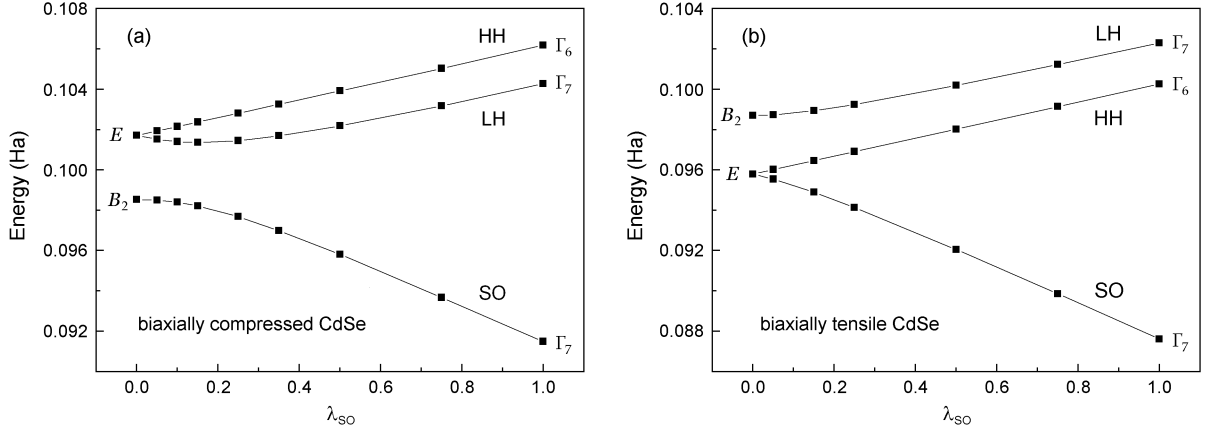


FIG. 1. Changes in energies of the valence subbands at  $\mathbf{k} = 0$  upon the adiabatic turning on the spin-orbit interaction in (a) biaxially compressed and (b) biaxially stretched CdSe crystals. The  $\lambda_{SO}$  scaling parameter denotes the portion of the spin-orbit interaction energy used in the calculations. The amount of strain is  $\pm 1\%$ .

tion of the  $|Z\rangle$  states in wave functions of a stretched sample decreases systematically but non-linearly, i.e. the mixing of the  $j = 1/2$  and  $j = 3/2$  states appears already at  $\mathbf{k} = 0$  (the symmetry of the  $D_{2d}$  group allows such mixing [26]). A decrease in the fraction of the  $j = 1/2, m_j = \pm 1/2$  states in the LH subband from 100% to 75% indicates that these states give the dominant contribution into this  $\Gamma_7$  band. This is a little bit surprising because the light holes are commonly associated with the  $j = 3/2, m_j = \pm 1/2$  states. On the contrary, the lowest band (denoted as SO), which genetically arises from the splitting of a doubly degenerate  $E$  band when the spin-orbit interaction is turned on, indicates its initial total angular momentum  $j = 3/2$ . As a result of mixing, at  $\lambda_{SO} = 1$ , this  $\Gamma_7$  symmetry band preserves the predominant fraction (75%) of the  $j = 3/2, m_j = \pm 1/2$  states, which is also surprising.

The changes in positions of the valence subbands at  $\mathbf{k} = 0$  as a function of strain are shown in Fig. 2. It is seen that without the spin-orbit interaction (thin black lines) a tetragonal strain always results in splitting of states with  $m = \pm 1$  and  $m = 0$  (as noted above, the latter state is a predecessor of the split-off band). When the spin-orbit interaction is turned on, the heavy holes band ( $\Gamma_6$ ) exhibits a parallel upward shift while the two remaining  $\Gamma_7$  bands undergo a complex interaction and mixing. The latter is evidenced by the observation of an anticrossing pattern characteristic of interacting bands with a minimum gap between the bands at a strain of  $\approx -1.37\%$ .

The fraction of  $|Z\rangle$  states in wave functions of the SO band as a function of biaxial strain is shown in Fig. 3. It is seen that the contribution of the  $|Z\rangle$  states into this band rapidly increases when the samples are compressed and rapidly decreases when the samples are stretched. As follows from the figure, this behavior is general for semiconductors with the zinc-blende structure. Accord-

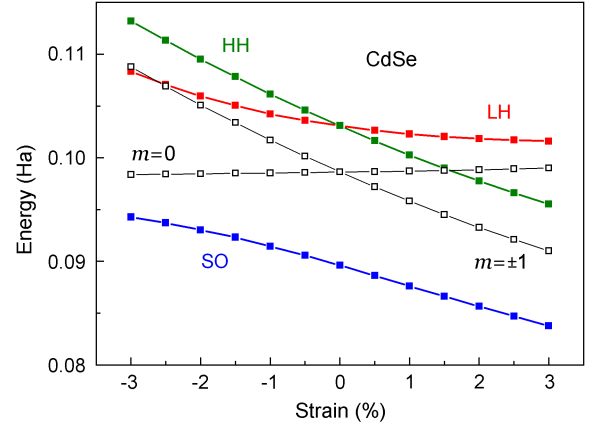


FIG. 2. Effect of the biaxial strain on the position of valence subbands at  $\mathbf{k} = 0$ . Thin black lines are the band energies without the spin-orbit interaction, color lines are the band energies when the spin-orbit interaction is taken into account.

ing to the results of analytical calculations carried out in Ref. [32] within the Kane model, the fraction of  $|Z\rangle$  states in the wave functions of this band is described by the equation

$$f_z = \frac{1}{2} \left( 1 - \frac{\Delta - 3S}{\sqrt{9\Delta^2 - 6S\Delta + 9S^2}} \right), \quad (4)$$

where  $S$  is the strain-induced splitting of the subbands of light and heavy carriers (without the spin-orbit interaction) and  $\Delta$  is the energy of spin-orbit splitting. The calculated dependence for CdSe is shown by a dashed line in Fig. 3; a qualitative agreement between the results of first-principles calculations and the predictions of the cited work is observed. The width of the transition region does indeed change approximately proportional to

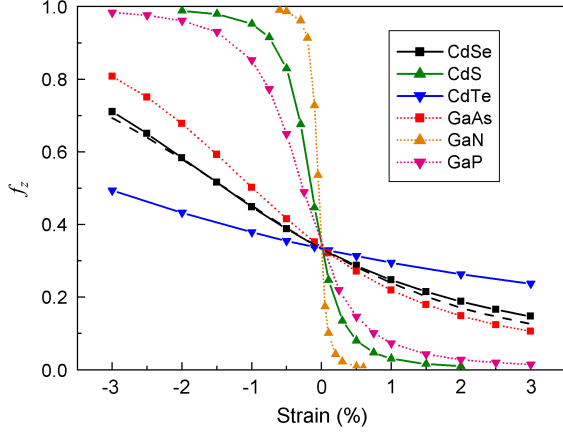


FIG. 3. Fraction of  $|Z\rangle$  states in the wave function of the SO subband as a function of biaxial strain for CdSe and several other bulk semiconductors with zinc-blende structure. The dashed line shows the results of fitting the calculated data for CdSe using Eq. (4).

the strength of the spin-orbit interactions. Note that the minimum gap between the LH and SO subbands falls on the strain value of  $\approx -1.37\%$ , at which the mixing of states in the indicated bands is maximal (in proportion 1:1).

### B. Matrix elements of optical transitions

The group theory states that for optical transitions to be allowed in the dipole approximation, the direct product of representations of groups describing the initial and final states should contain at least one vector representation. For the  $D_{2d}$  group we have  $\Gamma_6 \otimes \Gamma_6 = A_1 \oplus A_2 \oplus E$ ,  $\Gamma_6 \otimes \Gamma_7 = B_1 \oplus B_2 \oplus E$ ,  $\Gamma_7 \otimes \Gamma_7 = A_1 \oplus A_2 \oplus E$  [26]. This means that in the crystals under discussion, the  $\Gamma_6$ – $\Gamma_7$  optical transitions are allowed in both ( $\sigma$  and  $\pi$ ) polarizations, whereas the  $\Gamma_6$ – $\Gamma_6$  and  $\Gamma_7$ – $\Gamma_7$  transitions are allowed only in the  $\sigma$  polarization, in which the electric field vector lies in the  $xy$  plane.

By examining the scheme of possible optical transitions (Fig. 4), one can see that the only possible transition between the HH and CB bands is a transition in the  $\sigma$  polarization with a change of projection of the total angular momentum of  $\Delta m_j = \pm 1$ . The transition with  $\Delta m_j = \pm 2$  is forbidden in the dipole approximation, and the transition between the bands in the  $\pi$  polarization ( $\Delta m_j = 0$ ) are impossible because of the lack of a suitable final state in the conduction band.

For the LH→CB and SO→CB transitions, the identification of transitions is complicated by the equality  $|m_j| = 1/2$  for all involved states and the spin degeneracy of them at  $\mathbf{k} = 0$ . Although the transitions in  $\sigma$  and  $\pi$  polarizations can be distinguished by the values of matrix elements of the momentum operator  $|P_x|^2$

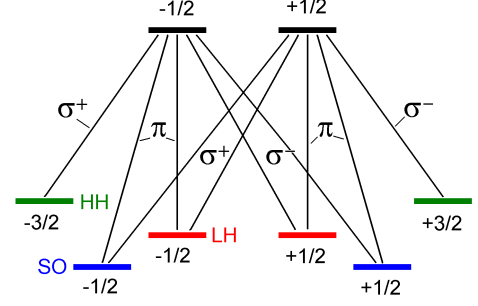


FIG. 4. Polarization of light accompanying direct interband optical transitions between states with different projections of the total angular momentum  $m_j$ .

and  $|P_z|^2$ , [35] the spin degeneracy results in a mixing of wave functions with  $m_j = 1/2$  and  $m_j = -1/2$  and does not allow unambiguous identification of all transitions. For their unambiguous identification, we used a trick with the imposition of an external magnetic field, which removes the degeneracy of these levels due to the Zeeman splitting. This allowed us to solve our problem. The only unresolved question was that the sign of the  $g$  factor in the Zeeman splitting remains unknown. If we take its sign to be positive for electrons, then the same sign applies for heavy holes, but the signs for other two bands are opposite to each other and depend on the strain. At a strain close to zero, the sign of the  $g$  factor for the SO band is positive while for the LH band it is negative. However, under strong biaxial compression, the signs of  $g$  factors for these bands are reversed. Curiously, the change in signs of  $g$  factors for these two bands occurs at approximately the same strain at which the contributions of the  $|Z\rangle$  states into the bands become equal. The results obtained with imposition of a magnetic field for the HHG pseudopotentials were completely confirmed by calculations with norm-conserving ONCVSP pseudopotentials [24] (we note that in the used version of the ABINIT program (8.10.3) such calculations are possible only for full-relativistic LDA pseudopotentials). The spin-resolved selection rules obtained within the described approach are in full agreement with the group-theoretical predictions.

The squares of the matrix elements of individual transitions in CdSe as a function of strain are shown in Fig. 5. At zero strain, the probabilities of individual transitions completely correspond to the probabilities expected for cubic crystals [36]. At non-zero strain, the probabilities of the LH→CB and SO→CB transitions are determined by the partial fractions of the  $|X\rangle$ ,  $|Y\rangle$ , and  $|Z\rangle$  states in the initial state, although these dependences are not exactly linear. The probability of transitions in the  $\pi$  polarization correlates with the fraction of  $|Z\rangle$  states in the wave function, and that for transitions in the  $\sigma$  polarization correlates with the fraction of  $|X \pm iY\rangle$  states in the wave function. It is interesting that despite

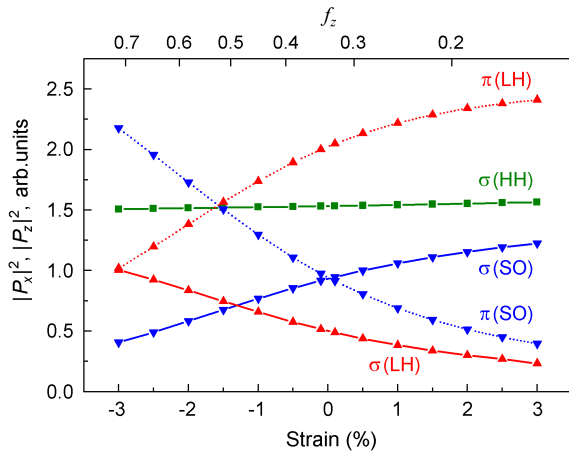


FIG. 5. Squares of matrix elements of optical transitions  $|P_x|^2$  and  $|P_z|^2$  as a function of biaxial strain of bulk CdSe. The top axis shows the fraction of the  $|Z\rangle$  states in the SO wave function.

strong changes in partial fractions of  $|X \pm iY\rangle$  and  $|Z\rangle$  states in the wave functions, the total intensity of the LH+SO $\rightarrow$ CB transitions as well as of the HH $\rightarrow$ CB one changes by no more than 3.5–4% over the entire strain range. These are only the intensities of individual components that are changed.

It is of interest to compare the obtained results with those obtained using the  $\mathbf{k} \cdot \mathbf{p}$  method. Unfortunately, no similar calculations were found for bulk CdSe, however, there are many publications devoted to similar calculations for cubic gallium nitride.

The results qualitatively consistent with ours were obtained in calculations of the matrix elements of HH $\rightarrow$ CB and LH $\rightarrow$ CB optical transitions in biaxially compressed and biaxially stretched GaN using the  $\mathbf{k} \cdot \mathbf{p}$  method [37].

On the other hand, similar calculations were carried out in Ref. [38] for multiple quantum wells from zincblende GaN biaxially compressed by 0.5% because of a contact with wide-gap AlGaIn layers. According to the authors' calculations, heavy holes make the main contribution to optical transitions in the  $\sigma$  polarization, and the total contribution of the LH and SO subbands are 6 times smaller. In the  $\pi$  polarization, the total contribution of the LH and SO subbands is approximately 2/3 of the contribution of heavy holes in the  $\sigma$  polarizations. The first question that arises is why the LH and SO bands are considered together. According to our calculations, at a biaxial strain of  $-0.5\%$  the splitting of these bands reaches 49 meV, and they must certainly be considered separately. Moreover, our calculations of the matrix elements of the momentum operator for GaN subjected to

the above strain give completely different relationships between the matrix elements. For example, the matrix elements of the HH $\rightarrow$ CB and LH $\rightarrow$ CB transitions in the  $\sigma$  polarization differs by only 1% while the SO $\rightarrow$ CB transitions in the  $\pi$  polarization should have approximately twice higher probability.

When calculating the matrix elements of the momentum operator, we observed that their values obtained using different functionals can differ markedly. For example, the value of the  $|P_x|^2$  matrix element for HH $\rightarrow$ CB transitions is 9.9 eV for PAW pseudopotentials, 14.9 eV for ONCVSP pseudopotentials, and 20.8 eV for HGH pseudopotentials. A comparison showed that the wave functions are sufficiently close to each other for HGH and ONCVSP pseudopotentials, whereas for PAW pseudopotentials they contain a strong background near the nuclei for the conduction band states. The value closest to the Kane energy used in the literature for CdSe (16.5 eV [18]) is obtained using the ONCVSP pseudopotentials.

## V. CONCLUSIONS

An approach to analyzing the spinor wave functions that appear in the electronic structure calculations when taking the spin-orbit interaction into account is developed. It is based on the projection analysis of angular parts of wave functions onto irreducible representations of the point group and analysis of the evolution of the energy levels upon the adiabatic turning on the spin-orbit interaction. This approach makes it possible to determine the genesis of the spinor wave functions, calculate the fractions of different contributions to the mixing of these states, and thus unambiguously identify electronic states. It seems promising to further use this approach to identify electronic states in low-dimensional systems such as superlattices, nanoplatelets, and nanoheterostructures, in which the valence band states are strongly mixed, and their unambiguous identification is complicated by the appearance of a large number of minibands as a result of the size quantization.

## CONFLICT OF INTEREST

The author declares that he has no conflict of interest.

## ACKNOWLEDGMENTS

This work was partly supported by the Russian Science Foundation grant No. 22-13-00101.

[1] E. O. Kane, The  $\mathbf{k} \cdot \mathbf{p}$  method, in *Semiconductors and Semimetals*, Vol. 1 (Academic Press, New York, London,

1966), Chap. 3, pp. 75–100.



- [2] L. C. Lew Yan Voon and M. Willatzen, *The  $\mathbf{k} \cdot \mathbf{p}$  Method. Electronic Properties of Semiconductors* (Springer-Verlag Berlin Heidelberg, 2009).
- [3] P.-O. Löwdin, A note on the quantum-mechanical perturbation theory, *J. Chem. Phys.* **19**, 1396 (1951).
- [4] D. M. Wood and A. Zunger, Successes and failures of the  $\mathbf{k} \cdot \mathbf{p}$  method: A direct assessment for GaAs/AlAs quantum structures, *Phys. Rev. B* **53**, 7949 (1996).
- [5] H. Fu, L.-W. Wang, and A. Zunger, Applicability of the  $\mathbf{k} \cdot \mathbf{p}$  method to the electronic structure of quantum dots, *Phys. Rev. B* **57**, 9971 (1998).
- [6] A. Zunger, How to describe the electronic structure of semiconductor quantum dots, in *Quantum Confinement V: Nanostructures*, Vol. 98-19, edited by M. Cahay, D. J. Lockwood, J. P. Leburton, and S. Bandyopadhyay (The Electrochemical Society, 1999), pp. 259–269.
- [7] L.-W. Wang and A. Zunger, High-energy excitonic transitions in CdSe quantum dots, *J. Phys. Chem. B* **102**, 6449 (1998).
- [8] L.-W. Wang and A. Zunger, Pseudopotential-based multiband  $\mathbf{k} \cdot \mathbf{p}$  method for  $\sim 250000$ -atom nanostructure system, *Phys. Rev. B* **54**, 11417 (1996).
- [9] M. Iraola, J. L. Mañes, B. Bradlyn, M. K. Horton, T. Neupert, M. G. Vergniory, and S. S. Tsirkin, IrRep: Symmetry eigenvalues and irreducible representations of *ab initio* band structures, *Comput. Phys. Commun.* **272**, 108226 (2022).
- [10] V. I. Klimov, ed., *Nanocrystal Quantum Dots* (CRC Press, Taylor & Francis Group, Boca Raton, London, New York, 2010).
- [11] D. Bera, L. Qian, T.-K. Tseng, and P. H. Holloway, Quantum dots and their multimodal applications: A review, *Materials* **3**, 2260 (2010).
- [12] B. T. Diroll, B. Guzelturk, H. Po, C. Dabard, N. Fu, L. Makke, E. Lhuillier, and S. Ithurria, 2D II–VI semiconductor nanoplatelets: From material synthesis to optoelectronic integration, *Chem. Rev.* **123**, 3543 (2023).
- [13] D. J. Stukel, R. N. Euwema, T. C. Collins, F. Herman, and R. L. Kortum, Self-consistent orthogonalized-plane-wave and empirically refined orthogonalized-plane-wave energy-band models for cubic ZnS, ZnSe, CdS, and CdSe, *Phys. Rev. B* **179**, 740 (1969).
- [14] M.-Z. Huang and W. Y. Ching, Calculation of optical excitations in cubic semiconductors. I. Electronic structure and linear response, *Phys. Rev. B* **47**, 9449 (1993).
- [15] Y. D. Kim, M. V. Klein, S. F. Ren, Y. C. Chang, H. Luo, N. Samarth, and J. K. Furdyna, Optical properties of zinc-blende CdSe and  $\text{Zn}_x\text{Cd}_{1-x}\text{Se}$  films grown on GaAs, *Phys. Rev. B* **49**, 7262 (1994).
- [16] A. H. Reshak, Theoretical investigation of the electronic properties, and first and second harmonic generation for cadmium chalcogenide, *J. Chem. Phys.* **124**, 104707 (2006).
- [17] A. H. Reshak, I. V. Kityk, R. Khenata, and S. Auluck, Effect of increasing tellurium content on the electronic and optical properties of cadmium selenide telluride alloys  $\text{CdSe}_{1-x}\text{Te}_x$ : An *ab initio* study, *J. Alloys Comp.* **509**, 6737 (2011).
- [18] S. Ithurria, M. D. Tessier, B. Mahler, R. P. S. M. Lobo, B. Dubertret, and A. L. Efros, Colloidal nanoplatelets with two-dimensional electronic structure, *Nat. Mater.* **10**, 936 (2011).
- [19] R. B. Vasiliev, A. I. Lebedev, E. P. Lazareva, N. N. Shlenskaya, V. B. Zaytsev, A. G. Vitukhnovskiy, Y. Yao, and K. Sakoda, High-energy exciton transitions in quasi-two-dimensional cadmium chalcogenide nanoplatelets, *Phys. Rev. B* **95**, 165414 (2017).
- [20] S. Bose, Z. Song, W. J. Fan, and D. H. Zhang, Effect of lateral size and thickness on the electronic structure and optical properties of quasi two-dimensional CdSe and CdS nanoplatelets, *J. Appl. Phys.* **119**, 143107 (2016).
- [21] X. Gonze, B. Amadon, P.-M. Anglade, J.-M. Beuken, F. Bottin, P. Boulanger, F. Bruneval, D. Caliste, R. Caracas, M. Côté, T. Deutsch, L. Genovese, P. Ghosez, M. Giantomassi, S. Goedecker, D. R. Hamann, P. Hermet, F. Jollet, G. Jomard, S. Leroux, M. Mancini, S. Mazevet, M. J. T. Oliveira, G. Onida, Y. Pouillon, T. Rangel, G.-M. Rignanese, D. Sangalli, R. Shaltaf, M. Torrent, M. J. Verstraete, G. Zerah, and J. W. Zwanziger, ABINIT: First-principles approach to material and nanosystem properties, *Comput. Phys. Commun.* **180**, 2582 (2009).
- [22] K. F. Garrity, J. W. Bennett, K. M. Rabe, and D. Vanderbilt, Pseudopotentials for high throughput DFT calculations, *Comput. Mater. Sci.* **81**, 446 (2014).
- [23] C. Hartwigsen, S. Goedecker, and J. Hutter, Relativistic separable dual-space Gaussian pseudopotentials from H to Rn, *Phys. Rev. B* **58**, 3641 (1998).
- [24] D. R. Hamann, Optimized norm-conserving Vanderbilt pseudopotentials, *Phys. Rev. B* **88**, 085117 (2013).
- [25] F. Ricci, S. Prokhorenko, M. Torrent, M. J. Verstraete, and E. Bousquet, Density functional perturbation theory within noncollinear magnetism, *Phys. Rev. B* **99**, 184404 (2019).
- [26] S. L. Altmann and P. Herzig, *Point-Group Theory Tables* (Clarendon Press, 1994).
- [27] G. L. Bir and G. E. Pikus, *Symmetry and Strain-induced Effects in Semiconductors* (John Wiley & Sons, New York, 1974).
- [28] J. M. Luttinger and W. Kohn, Motion of electrons and holes in perturbed periodic fields, *Phys. Rev.* **97**, 869 (1955).
- [29] G. Dresselhaus, Spin-orbit coupling effects in zinc blende structures, *Phys. Rev.* **100**, 580 (1955).
- [30] E. O. Kane, Band structure of indium antimonide, *J. Phys. Chem. Solids* **1**, 249 (1957).
- [31] S. L. Chuang, *Physics of Optoelectronic Devices* (John Wiley & Sons, Inc., 1995).
- [32] G. Jones and E. P. O'Reilly, Improved performance of long-wavelength strained bulk-like semiconductor lasers, *IEEE J. Quant. Electron.* **29**, 1344 (1993).
- [33] Due to the absence of an inversion center in crystals with the  $D_{2d}^9$  space group, the spinor wave functions are described by two independent components at all points of the Brillouin zone except for the  $\Gamma$ ,  $X$ ,  $M$  points and the points on the  $\Lambda$  axis.
- [34] Such calculations can be performed in the ABINIT program, in which the portion of the spin-orbit interaction energy used in the calculations with PAW pseudopotentials,  $\lambda_{\text{SO}}$ , is controlled by the `spnorb` variable.
- [35] To do this, we need a tetragonal strain; without it, the matrix elements in all polarizations are the same (cubic symmetry).
- [36] M. I. Dyakonov and V. I. Perel, Theory of optical spin orientation of electrons and nuclei in semiconductors, in *Optical Orientation*, edited by F. Meier and B. P. Zakharchenya (Elsevier Science Publisher B. V., 1984), Chap. 2, pp. 11–71.



- [37] S. J. Yoon and I. Lee, Tensile strain effects on GaN-based quantum well lasers, J. Korean Phys. Soc. **34**, S386 (1999).
- [38] W. J. Fan, M. F. Li, T. C. Chong, and J. B. Xia, Valence hole subbands and optical gain spectra of GaN/Ga<sub>1-x</sub>Al<sub>x</sub>N strained quantum wells, J. Appl. Phys. **80**, 3471 (1996).